Electronic Supplementary Information (ESI)

One-step Electrosynthesis of Visible Light Responsive Double-walled Alloy Titanium Dioxide Nanotube Arrays for Use in Photocatalytic Degradation of Dibutyl Phthalate

*Yuan Wang,[a] Xueke Zhang,[a] Suzhen You[a] and Yun Hu *[a,b,c]*

[a] School of Environment and Energy, South China University of Technology, Guangzhou 510006, P. R. China

[b] Guangdong Provincial Key Laboratory of Atmospheric Environment and Pollution Control, Guangzhou 510006, PR China

[c] The Key Lab of Pollution Control and Ecosystem Restoration in Industry Clusters, Ministry of Education, Guangzhou 510006, P. R. China

*Corresponding author. Tel: +86-020-3938-0573, E-mail: huyun@scut.edu.cn

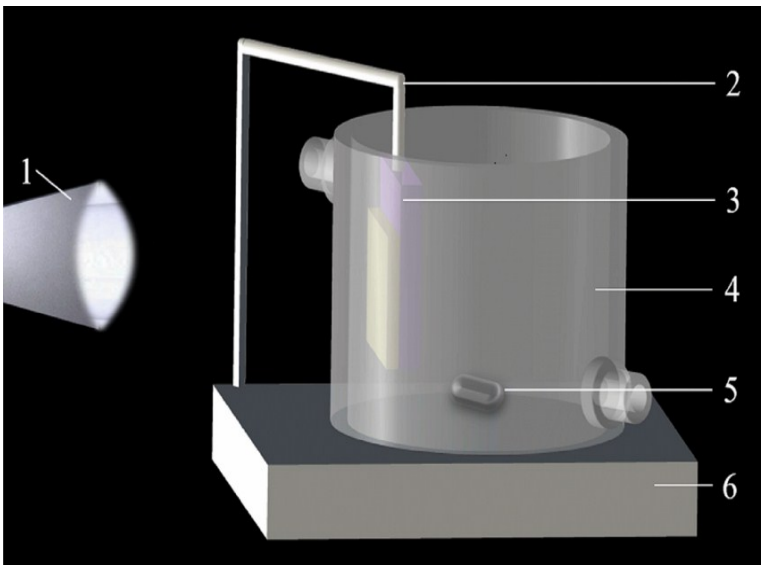

Fig. S1. The self-made photocatalytic reactor: (1) xenon lamp light source, (2) photocatalyst support frame, (3) photocatalyst, (4) circulating jacket reactor, (5) rotor, and (6) beater.

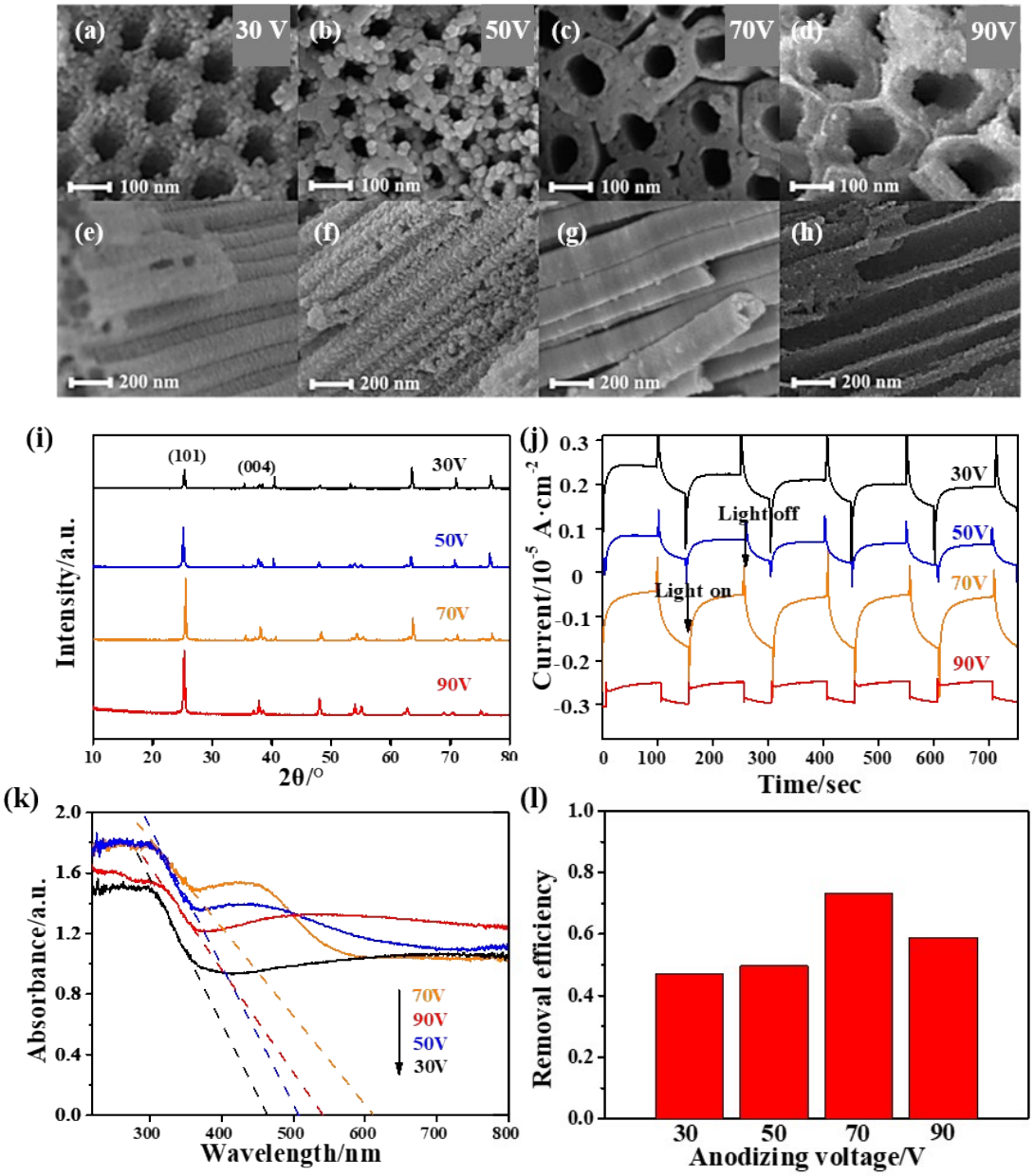

Fig. S2. The top and lateral view SEM images of ATNTAs with different anodization voltage: 30 V (a, b), 50 V (c, d), 70 V (e, f), 90 V (g, h); the (i) XRD patterns, (j) I-t curve, (k) UV-vis DRS and (l) DBP removal efficiency of ATNTAs with different anodization voltage under visible light irradiation. Other anodization conditions of samples are use a 0.5 wt% NH_4F-2 vol% H_2O electrolyte, for 2 h.

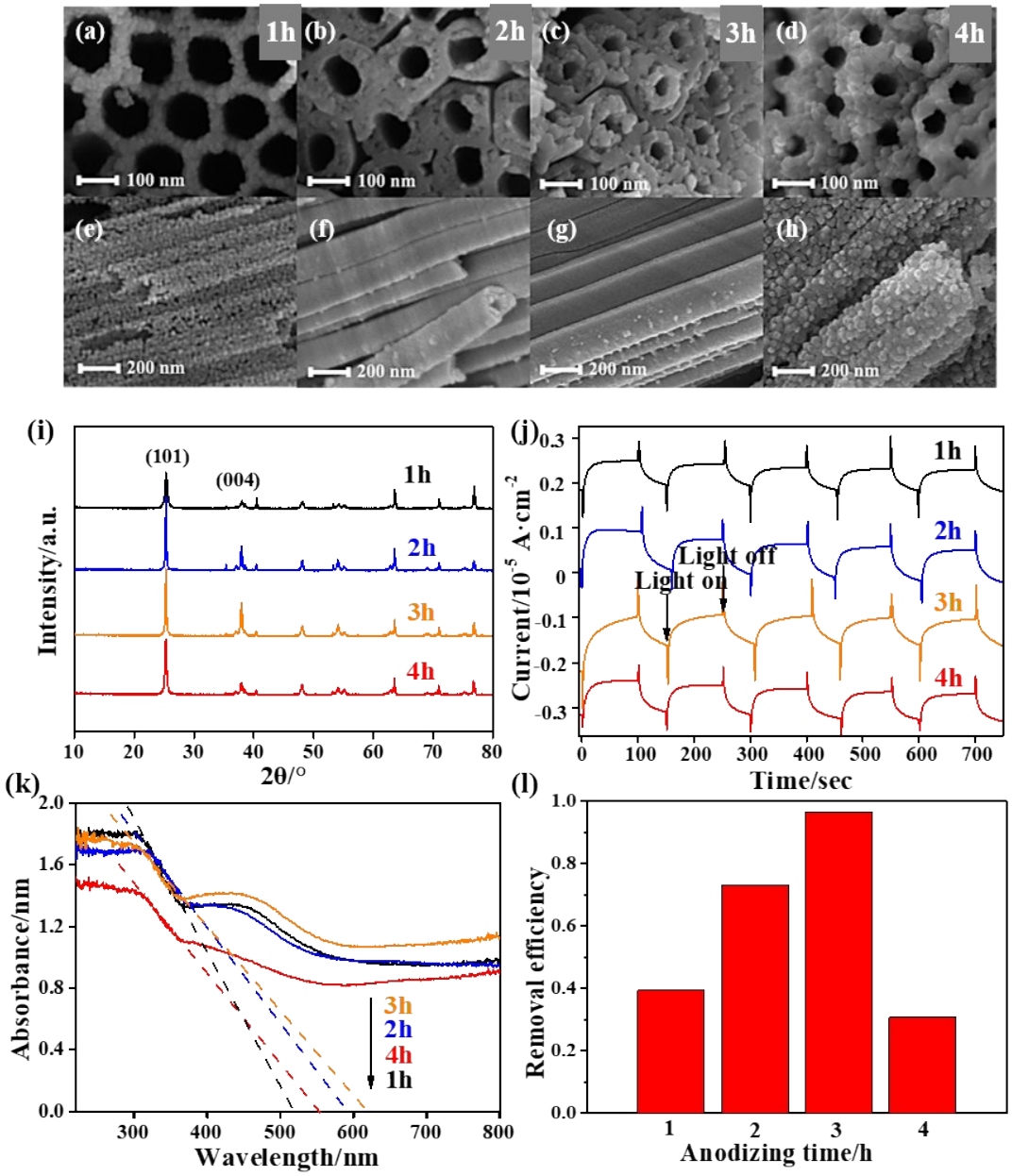

Fig. S3. The top and lateral view SEM images of ATNTAs with different anodization time: 1 h (a, b), 2 h (c, d), 3 h (e, f), 4 h (g, h); the (i) XRD patterns, (j) I-t curve, (k) UV-vis DRS and (l) DBP removal efficiency of ATNTAs with different anodization time under visible light irradiation. Other anodization conditions of samples are a voltage of 70 V, and using a 0.5 wt% NH_4F-2 vol% H_2O electrolyte.

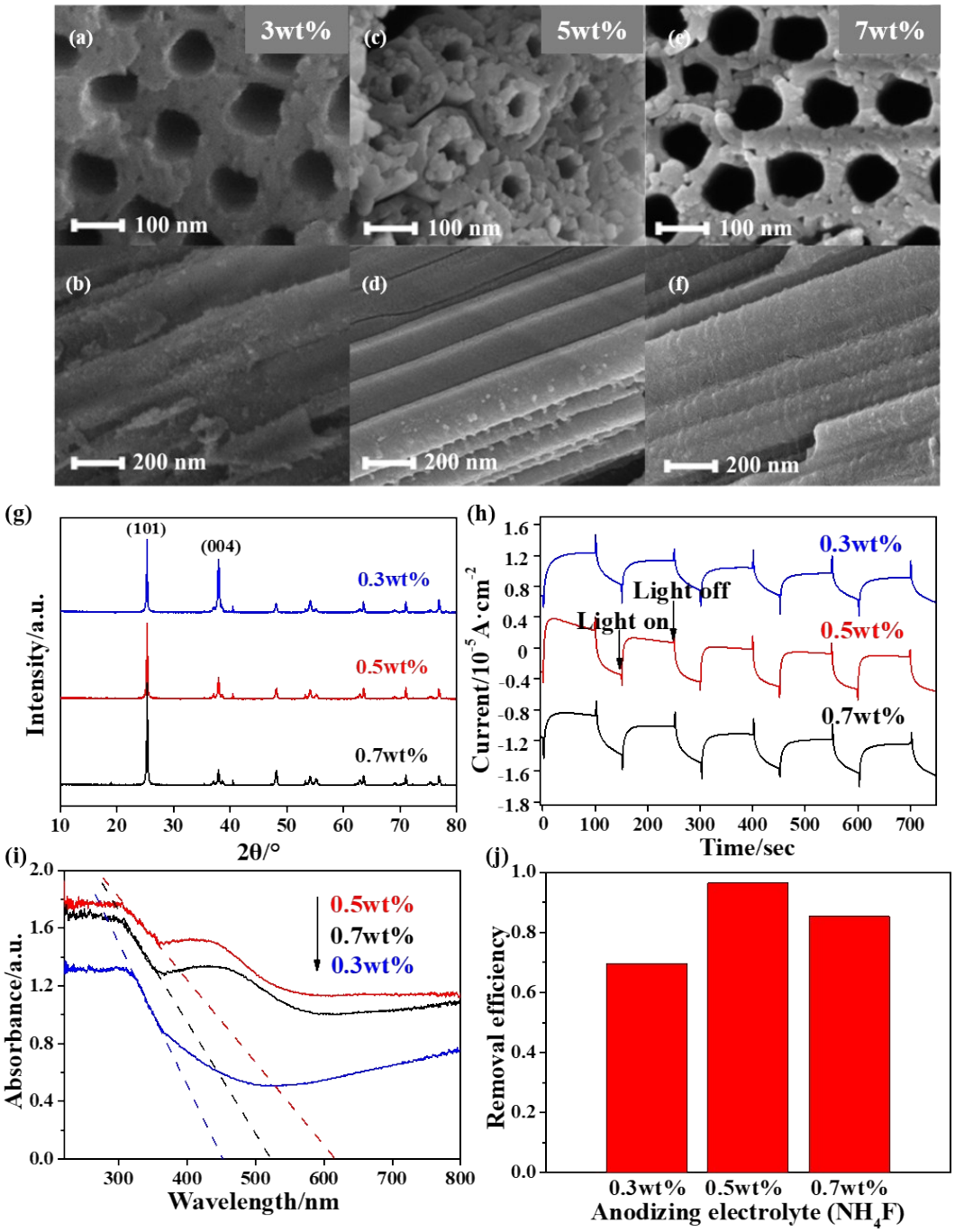

Fig. S4. The top and lateral view SEM images of ATNTAs made in different NH_4F concentration of anodization electrolyte: 3 wt% (a, b), 5 wt% (c, d), 7 wt% (e, f); the (g) XRD patterns, (h) I-t curve, (i) UV-vis DRS and (j) DBP removal efficiency of ATNTAs made in different NH_4F concentration of anodization electrolyte under visible light irradiation. Other anodization conditions of samples are a voltage of 70 V, for 3 h, and using a 2 vol% H_2O electrolyte.

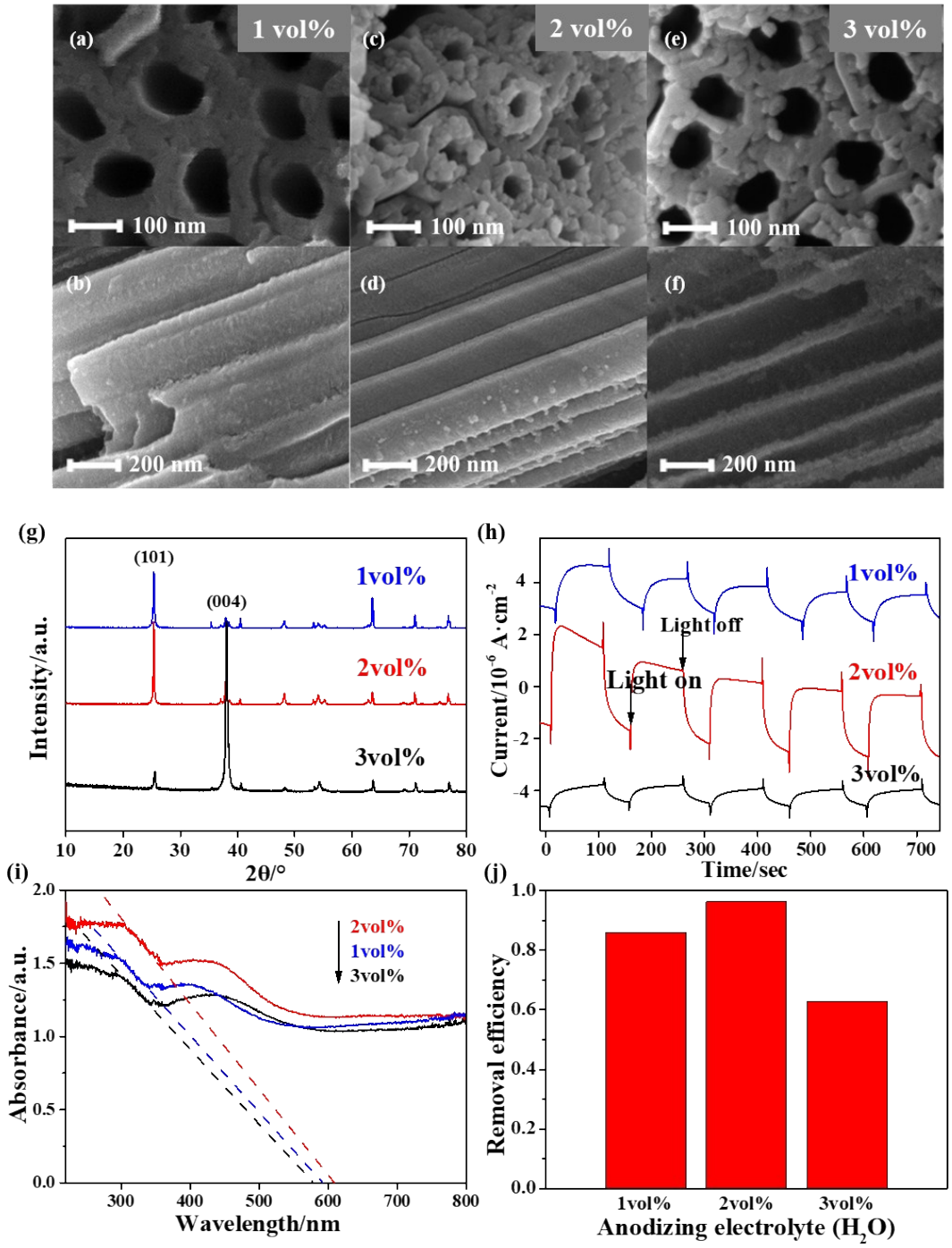

Fig. S5. The top and lateral view SEM images of ATNTAs made in different H_2O concentration of anodizing electrolyte: 1 vol% (a, b), 2 vol% (c, d), 3 vol%(e, f); the (g) XRD patterns, (h) I-t curve, (i) UV-vis DRS and (j) DBP removal efficiency of ATNTAs made in different H_2O concentration of anodizing electrolyte under visible light irradiation. Other anodization conditions of samples are a voltage of 70 V, for 3 h, and using a 0.5 wt% NH_4F electrolyte.

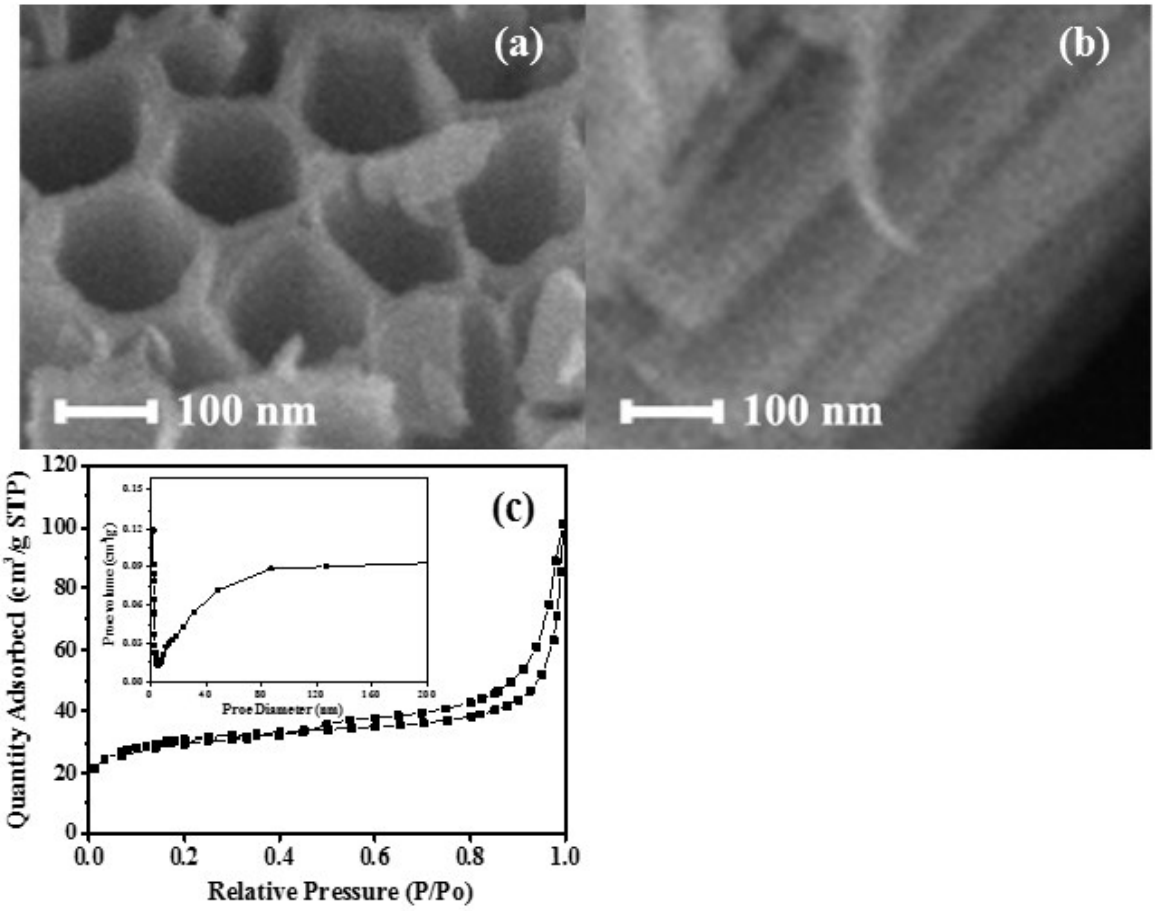

Fig. S6. The(a) top and (b) side view of SEM images and (c) N_2 adsorption/desorption isotherm with inset of pore size distribution of DW-ATNTAs before calcination.

Table S1. Porous parameters of DW-ATNTAs before and after calcination.

	S_{BET} (m^2/g)	V_p (cm^3/g)	D_p (nm)
Before Calcination	65.63	0.16	6.45
After Calcination	91.08	0.26	16.07

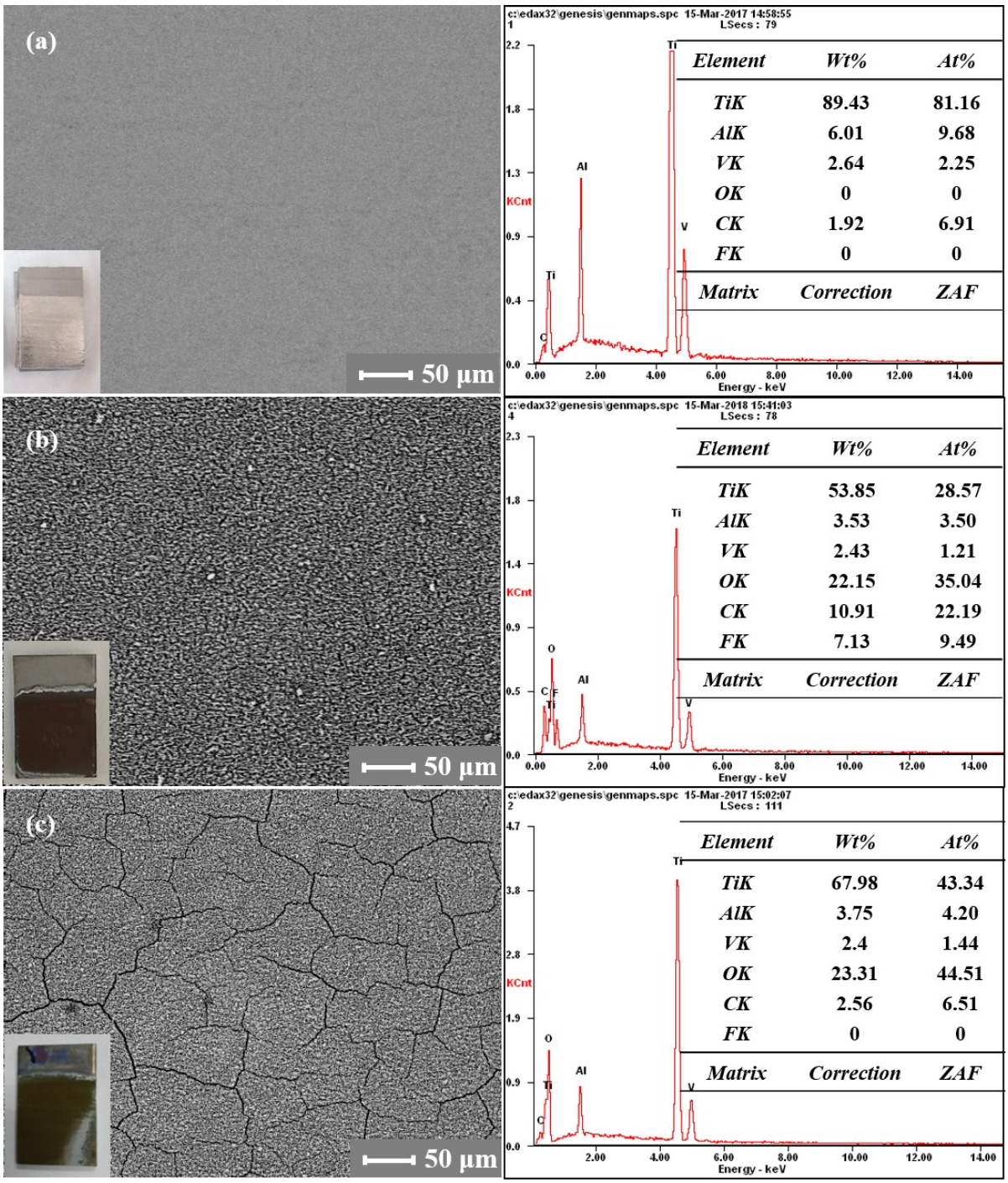

Fig. S7. The EDX analysis of DW-ATNTAs: (a) before and (b) after anodization; (c) after calcination.

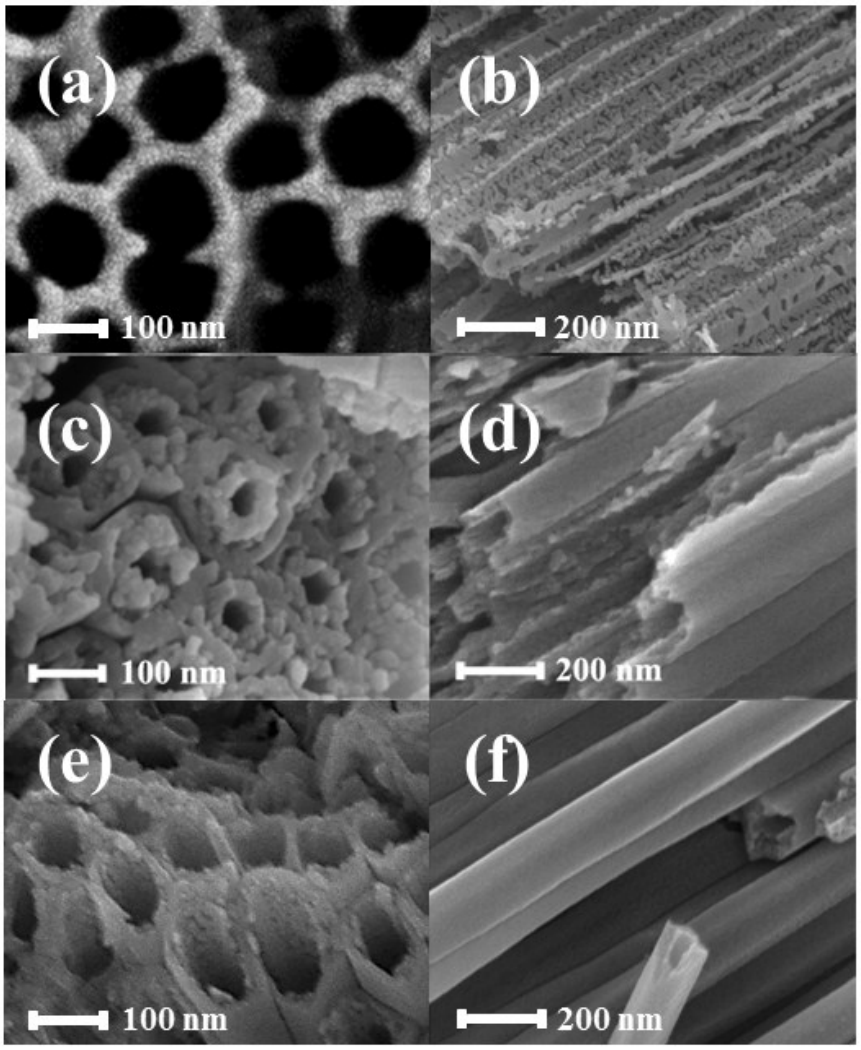

Fig. S8. The SEM images of different ATNTAs: (a) top and (b) side view of 3Al-SW-ATNTAs, (c) top and (d) side view of DW-ATNTAs, (e) top and (f) side view of 6Al6V-DW-ATNTAs.

3Al-SW-ATNTAs signified nanotube arrays on TA28 (3Al) alloy. Fig. S8a, b shows the morphologies of 3Al-SW-ATNTAs with a diameter of 180 nm and a thickness of 20 nm. The tube wall is not separated with others and has seriously erosion phenomenon, so it appears as a single-walled porous nanotube array in the form of particle accumulation. DW-ATNTAs signified nanotube arrays on TC4 (6Al4V) alloy. From the top and side view of DW-ATNTAs in Fig. S8c, d, it can be clearly seen that doubled-walled nanotube arrays were fabricated. The outer wall is relatively smooth with the diameter of 180 nm and the thickness of 20 nm, while the inner wall is porous with the diameter of 100 nm and the thickness of 20 nm by anti-erosion ability. 6Al6V-DW-ATNTAs signified nanotube arrays on TC10 (6Al6V) alloy. The top and side view of 6Al6V-DW-ATNTAs in Fig. S8e, f show that the doubled-walled nanotube arrays were fabricated. The outer wall is smooth with the diameter of 180 nm and the thickness of 20 nm, while the inner wall has slightly erosion phenomenon with the diameter of 120 nm and the thickness of 10 nm by particle accumulation.

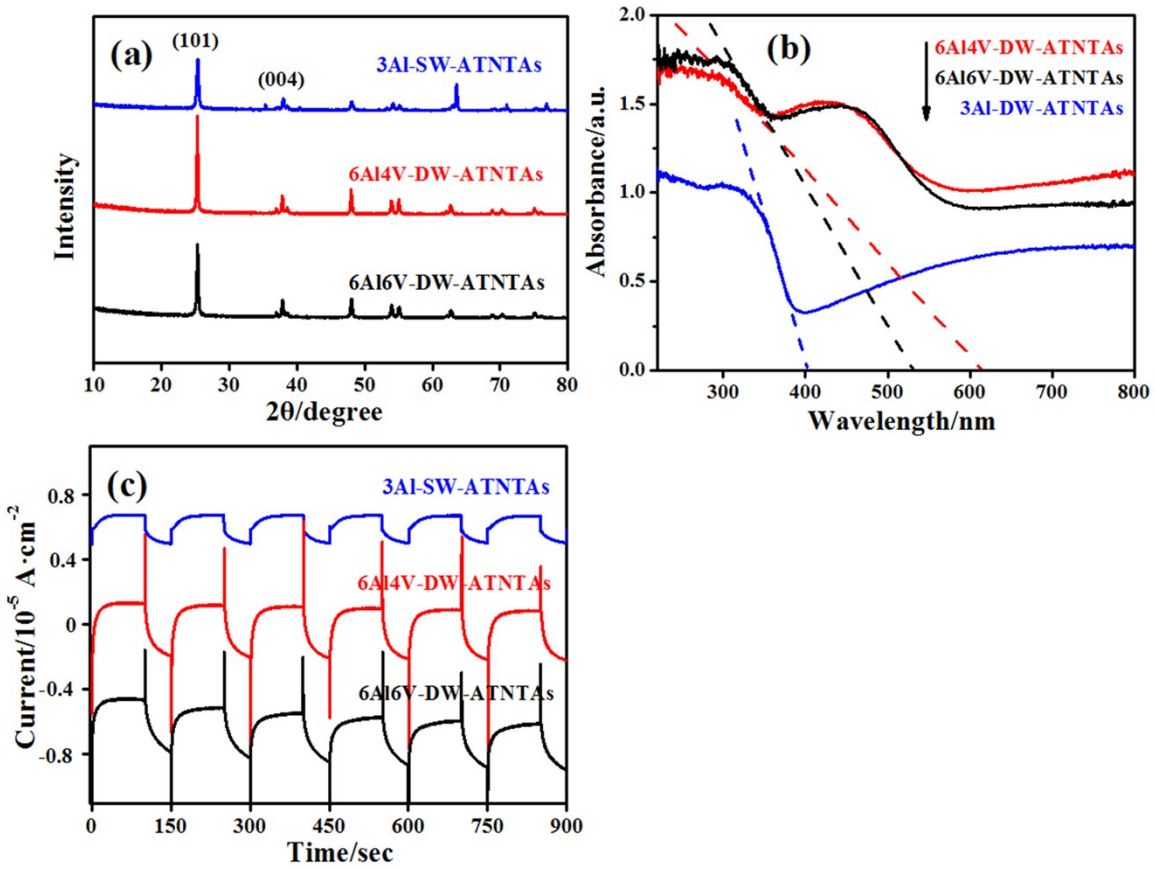

Fig. S9. The (a)XRD patterns, (b) UV-vis DRS, (c) i-t curve of different ATNTAs.

The XRD analysis (Fig. S9a) show that all of the ATNTAs are anatase phase TiO_2. The Fig. S9b show the UV-Vis DRS spectra of different photocatalysts, in which 3Al-SW-ATNTAs is 401 nm, 6Al6V-DW-ATNTAs is 607 nm, and 6Al6V-DW-ATNTAs is 530 nm, and the calculated forbidden band widths are: 3.09, 2.04, and 2.34 eV, respectively. The transient photocurrent curves of ATNTAs in Fig. S9c show that the DW-ATNTAs has the highest photocurrent. This observation shows that V element is the main factor affecting the visible light performance of the catalyst. The different ATNTAs displays stable current responses under visible light irradiation. Their response values are in the order of 6Al4V-DW-ATNTAs＞6Al6V-DW-ATNTAs＞3Al-SW-ATNTAs. However, 6Al6V-DW-ATNTAs do not show the better photo-response than 6Al4V-DW-ATNTAs, which is attributed to the fact that 6Al6V-DW-ATNTAs is more easily to be corroded and more seriously losses of V element.

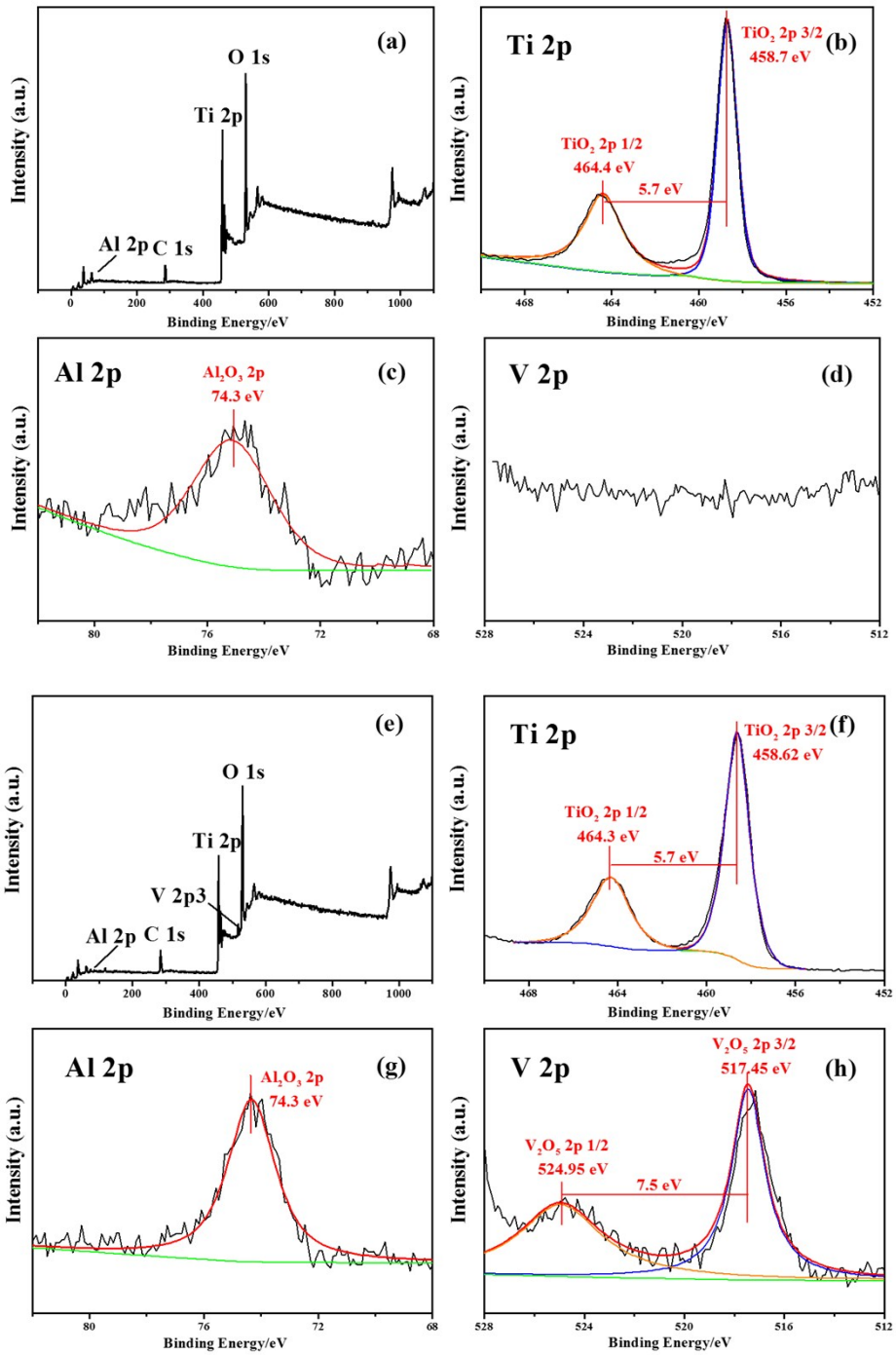

Fig. S10. The high resolution XPS patterns of 3Al-SW-ATNTAs (a) survey (b)Ti 2p(c)Al 2p (d)V 2p; of 6Al6V-DW-ATNTAs (e) survey (f)Ti 2p(g)Al 2p (h)V 2p.

Different ATNTAs were characterized by XPS, as shown in Fig. 5 and Fig. S10. Fig. S10a was the full scan spectra of 3Al-SW-ATNTAs, shows that the mainly elements exist in the catalysts were Ti, O and Al. There is no relative shift in the peak of the corresponding elements (Fig. S10b, c, d), which proves that the elements exist independently in 3Al-SW-ATNTAs in the form of oxides. Similarly, Fig. S10e showed that 6Al6V-DW-ATNTAs mainly contains Ti, O, Al and V elements, which are independently present as oxides such as TiO_2, Al_2O_3, and V_2O_5 (Fig. S10f, g, h).

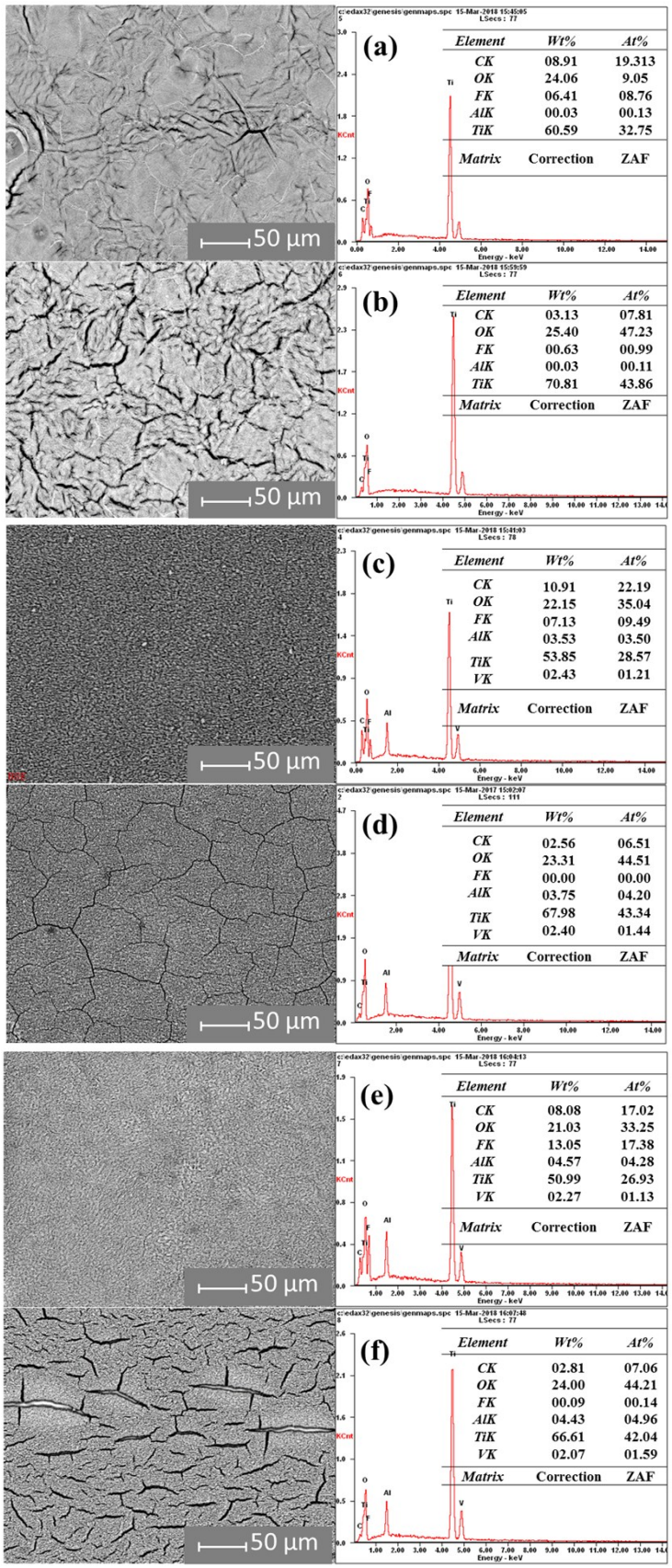

Fig. S11. The EDX analysis of different ATNTAs: 3Al-SW-ATNTAs (a) before and (b) after calcination; 6Al4V-DW-ATNTAs (c) before and (d) after calcining; 6Al6V-DW-ATNTAs (e) before and (f) after calcination.

Table S2. The element content variation of ATNTAs during formation process.

Element /wt%	TA28 (3Al-SW-ATNTAs)			TC4 (6Al4V-DW-ATNTAs)			TC10 (6Al6V-DW-ATNTAs)		
	Before Anodization	After Anodization	After Calcination	Before Anodization	After Anodization	After Calcination	Before Anodization	After Anodization	After Calcination
Ti	96.98	60.59	70.81	89.43	53.85	67.98	87.66	50.99	66.61
Al	02.94	00.03	00.03	06.01	03.53	03.75	06.37	04.57	04.43
V	0	0	0	02.64	02.43	02.40	05.44	02.27	02.07
O	0	24.06	25.40	0	22.15	23.31	0	21.03	24.00
C	00.08	08.91	03.13	01.92	10.91	02.56	00.53	08.08	02.80
F	0	06.41	00.63	0	07.13	0	0	13.05	00.09

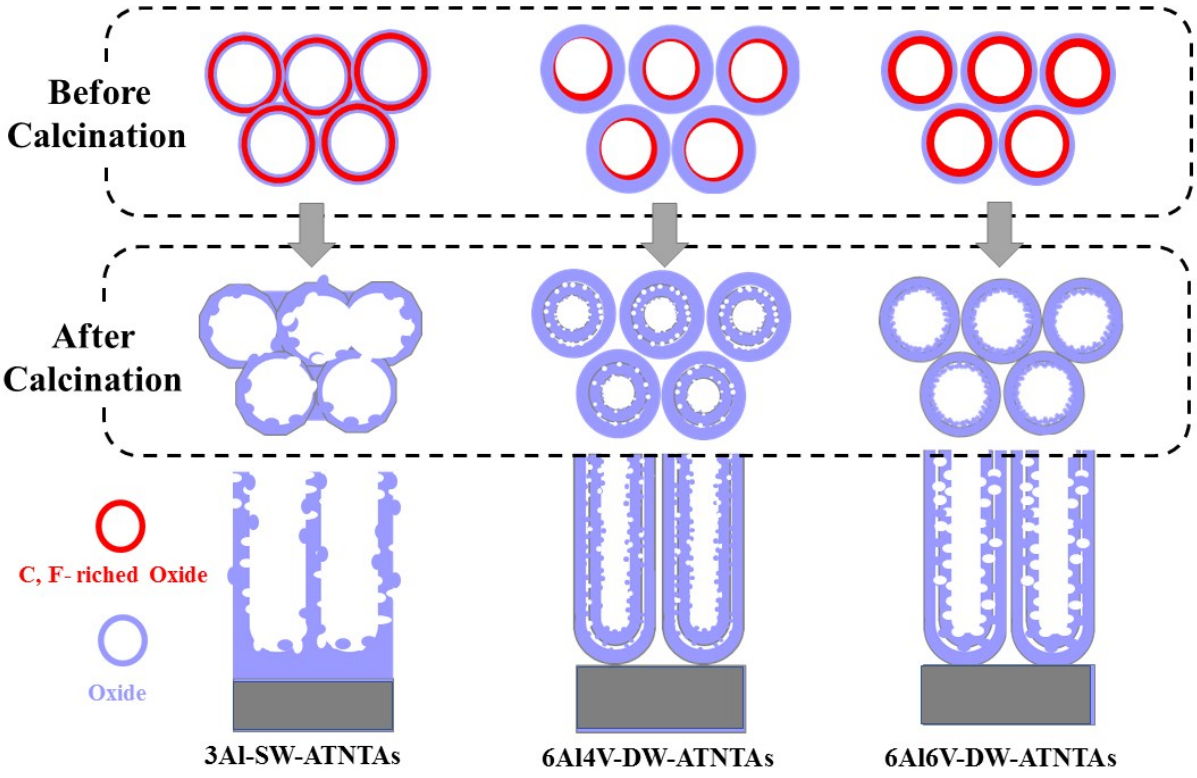

Fig. S12. The formation schematic of different morphology ATNTAs.

Table S3. Comparison of the reaction rate constant with reported in literatures.

Reference	Material	Method	Photocatalytic performance
This work	Double-walled alloy TiO_2 nanotube arrays with porous inner wall	Anodization method	50 times (TiO_2) 7 times ($A/TiO_{2(plate)}$)
Appl. Catal. B: Environ. 250 (2019) 301-312.	Mesoporous TiO_2 nanotubes	Dual-template method	9.8 times (TiO_2) 3.6 times (P25)
Appl. Catal. B: Environ. 263 (2020) 118353.	PbO-decorated TiO_2 nanocubes	Hydrothermal and thermal treatment	33.2 times (TiO_2)
Chem. Eng. J. 296 (2016) 420-427	TiO_2 nanorods	Hydrothermal and thermal treatment	1.2 times (P25)
Chem. Eng. J. 377 (2019) 120087.	WO_3-doped TiO_2	Liquid phase plasma method	6.7 times (TiO_2)
Environ. Sci. Technol. 50 (2016) 2556-563	TiO_2 nanotubes	Anodization method	1.1 times (P25) [a]

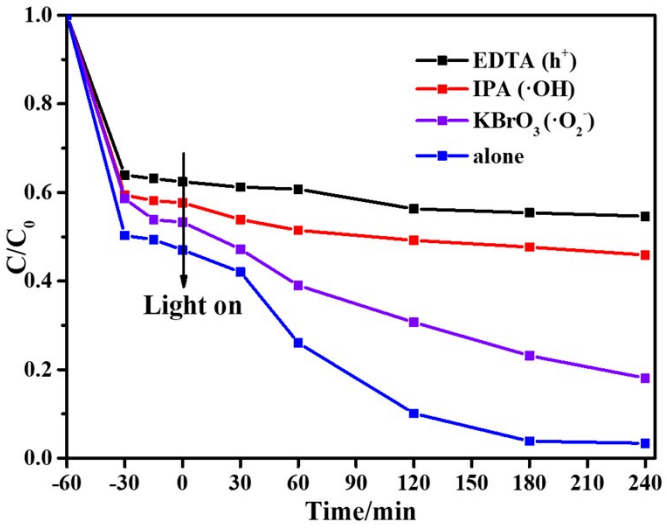

Fig. S13. The photocatalytic degradation of DBP over DW-ATNTAs with different scavengers under visible light irradiation.